X-615-65-304

NASA TM X-55318

THE LOWER IONOSPHERE AT SOLAR MINIMUM

BY

R. E. BOURDEAU

A. C. AIKIN

J. L. DONLEY

JULY 1965

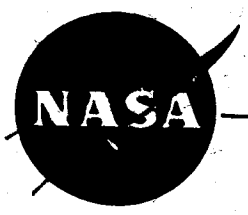

GODDARD SPACE FLIGHT CENTER

GREENBELT, MARYLAND

Ionospheric Physics Preprint Series
To be published in the Journal of Geophysical Research

THE LOWER IONOSPHERE AT SOLAR MINIMUM

by

R. E. Bourdeau, A. C. Aikin and J. L. Donley
Space Sciences Division
NASA-Goddard Space Flight Center
Greenbelt, Maryland

ABSTRACT

Two Nike-Apache rockets were launched in 1964 to measure: (a) positive ion density (N_+) with an altitude resolution of approximately 10 meters by use of a modified Gerdien condenser, (b) electron density by radio-propagation techniques and (c) the optical depth of solar radiation absorbed in the 60-120 km region with a photoelectron retarding potential analyzer. The flights took place at a time when the intensities of important portions of the solar spectrum were being measured simultaneously from a satellite. The simultaneity of all these data and the high altitude resolution of the charged particle density profiles permits us to identify several regions between 65 and 120 km and to associate them with different portions of the solar spectrum and with different loss mechanisms.

The average N_+ in the D region (65-83 km) is found to be $10^3 cm^{-3}$, an order of magnitude less than reported by investigators who used experiments which unlike ours require assumptions about other ionic parameters to derive N_+. The profile in this region is consistent with Lyman alpha ionization of nitric oxide whose abundance is computed to be approximately $3x10^{-10}$ that of molecular oxygen and with an effective positive ion loss rate of approximately $2x10^{-8} cm^3 sec^{-1}$.

The regions 83-88 km and 88-93 km are sequentially ionized by 2-8Å X-radiation and the C VI line at 33.7Å which produce O_2^+ and N_2^+ ions. These ions are trans-

formed into NO^+ by processes involving charge transfer and/or ion-atom interchange ($N_2^+ + O_2 \rightarrow O_2^+ + N_2 \rightarrow NO^+ + NO$). From our results, we compute the effective loss rate between 83-93 km to be approximately $2 \times 10^{-8} cm^3 sec^{-1}$ which quite likely represents the dissociative recombination rate for NO^+.

The region 95-115 km is ionized principally by extreme ultraviolet radiation leaving O_2^+ as one of the two dominant ions. Though never dominant, 40-75Å X-radiation is an important ionizing source which indirectly produces some NO^+ ions above 95 km through the process $N_2^+ + O \rightarrow NO^+ + N$. Our computed effective dissociative recombination rate between 95-115 km is about $1.8 \times 10^{-7} cm^3 sec^{-1}$. It is suggested that this value is higher than that computed for the region below 90 km because above 95 km the ionic content is richer in O_2^+.

INTRODUCTION

Existing theories for the formation of the D and lower E regions of the ionosphere are as yet incomplete. In the D region uncertainties in our knowledge principally of the density of the trace constituent, nitric oxide, and of both the nature and magnitude of the significant loss mechanisms prevent a determination of the relative importance of 2-8Å X-rays and Lyman alpha (1215.7Å) radiation. In the lower E region, uncertainties in the magnitude and spectral distribution of 30-100Å X-radiation have led to difficulties in assessing the importance of this wavelength band as compared to the spectral region 911-1027Å.

Additionally, there is no adequate explanation over the entire 83-120 km region for ion spectrometer measurements which show that N_2^+ is a trace ionic constituent even though

it has a high production rate and that NO^+ is an important ion even though it probably is not a direct photoionization product. Finally, there are differences of at least an order of magnitude in the effective loss rates for various theoretical models of both the D and E regions.

This paper examines all of these problems by computing production rates with the aid of simultaneous satellite measurements of X-radiation and rocket measurements of Lyman alpha optical depth. The production rates then are compared with rocket measurements of charged particle density to derive effective recombination coefficients for the 83-120 km region. This comparison is then interpreted in terms of recent laboratory measurements of ion-molecule reaction rates and ion spectrometer data. Finally, the recombination coefficients derived for 83-120 km are used to suggest a nitric oxide distribution important to theories of D region formation.

THE ION DENSITY EXPERIMENT

The experiment used to measure ion densities is a hybrid in that it combines the features of (a) the classical Gerdien condenser which has been used for many years by workers in atmospheric electricity and (b) the planar ion traps used for rocket and satellite investigations of the upper ionosphere. It basically consists of an open-ended cylinder mounted at the front end of the rocket with its axis parallel to the air flow. A small streamlined cylindrical probe is mounted in a recessed position at the center and concentric with the large cylinder. The outer cylinder is maintained at rocket potential while the inner probe is biased negatively to collect positive ions and to repel negatively-charged particles. The actual configuration includes the use of a large ratio of exit to aperture areas (Fig. 1) in order to minimize the shock wave effects.

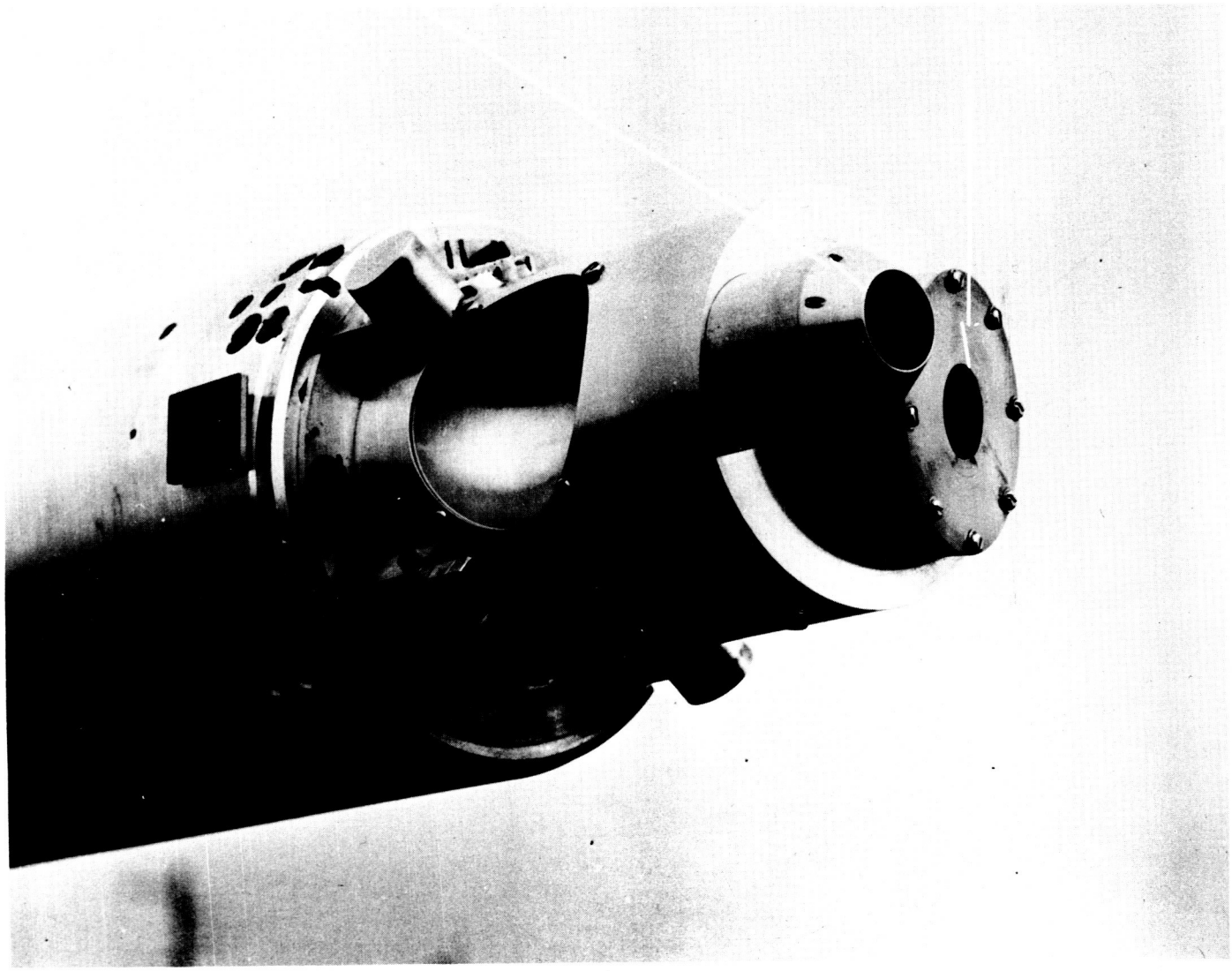

Figure 1. Photograph of Nike-Apache payload showing ion density and solar radiation experiment sensors.

These effects have been critically examined and found not to be significant even for the case of a rocket traveling at altitudes of relatively high pressures such as those found in the D region (Bourdeau et al, 1959).

In their use of a similar instrument on the ground, on aircraft and on balloons, workers in atmospheric electricity deal with the case where the short mean free path of the ions restricts the net distance that the ion travels even though its thermal velocity may be greater than the air flow velocity. For this case, the collector current will increase linearly with applied potential at low potential values. The slope of the volt-ampere curve in this region is a measure of the ionic conductivity. At a critical value of the collector potential which is dependent on the ratio of the air flow to the ion mobility, all of the ions entering the instrument are collected. For values of potential in excess of this critical value, the collector current (I_c) will have a saturation value which is independent of potential and is a measure of the ion density (N_+) according to:

$$I_c = N_+ e \; V_R \; A \cos \theta \qquad (1)$$

where e is the electronic charge, V_R is the rocket or air flow velocity, A is the area of the aperture, and θ is the angle between the cylinder axis and the direction of the air flow. Values of the critical potential as a function of altitude were computed for typical rocket velocities by Bourdeau et al (1959). According to these calculations, we comfortably should be dealing with saturation currents at all altitudes above 60 km for the fixed applied potential (20 volts) used in the present experiment. In the exploratory experiments, saturation currents were not observed, most

likely because the effective collection area of the instrument with its relatively exposed central electrode increased with applied potential (Bourdeau et al, 1959). To eliminate this possibility, the central electrode in the present experiment was recessed and shielding grids designed to contain the electric field due to the applied potential were mounted at the aperture and exit openings.

Workers in atmospheric electricity generally deal with one extreme use of the instrument - the case where the ion thermal velocity is greater than the airflow velocity. The use of the instrument at the other extreme where the airflow velocity is much greater than the ion random thermal velocity has been described by upper ionospheric investigators using rockets and satellites. It has been aptly demonstrated by agreement with results from an independent radio-propagation experiment flown on the same rocket (Bauer et al, 1964) that the ion current measured for this application is identically that given by equation (1). For all altitudes below 130 km in our experiments, the rocket velocity exceeded by at least a factor of two the ion random thermal velocity computed by assuming (a) a mean ionic mass of 30 AMU and (b) a temperature profile given by the US Standard Atmosphere.

Thus, identical expressions result from the extreme cases for which the ion density experiment has been used. This occurs because the same physical requirement is met - that the net distance travelled by the ion with respect to the medium is very small compared with the distance the ion is carried along by the medium in the same time interval. At D region altitudes, we are dealing with an intermediate case, one where the air flow velocity exceeds the ion velocity but where additionally the mean free paths are such that the ions can suffer collisions within the measuring

instrument. This case as well as the two extreme cases has been analyzed by Whipple (1963) who finds that equation (1) is still valid for the rocket and ion velocities expected here and for the ratios of mean free paths to the dimensions of our instrument.

The advantages of our experiment over others used to obtain D region ion densities are that it is relatively insensitive to (a) vehicle potential, (b) to unwanted photocurrent and (c) a knowledge of other ionic parameters to derive ion density. The photocurrent problem can be an especially serious one at D region altitudes. In one of the two rocket flights described here the photocurrent measured by an experiment described in a subsequent section exceeded the measured positive ion current by almost an order of magnitude at 75 km. We eliminated the problem for the ion density experiment by recessing the electrode to where it was not exposed to the sun. If an exposed probe had been used in this situation it would have to have an effective ion collection area which is an order of magnitude larger than the actual surface area in order to overcome the unwanted photocurrent.

CHARGED PARTICLE DENSITY RESULTS ($Z = 58^{o}$)

On one of the two rocket flights with which this report is concerned, positive ion density was measured by use of the experiment described in the previous section while the familiar Seddon CW propagation experiment was used for electron density (N_e) determination. The comparison of N_+ and N_e is important to the understanding of D region formation because of the possibility of electron loss through negative ion (N_-) formation such that $N_+ = N_e + N_-$.

The results of the simultaneous experiments are presented in Figure 2. The measured values of N_+ and N_e are in agree-

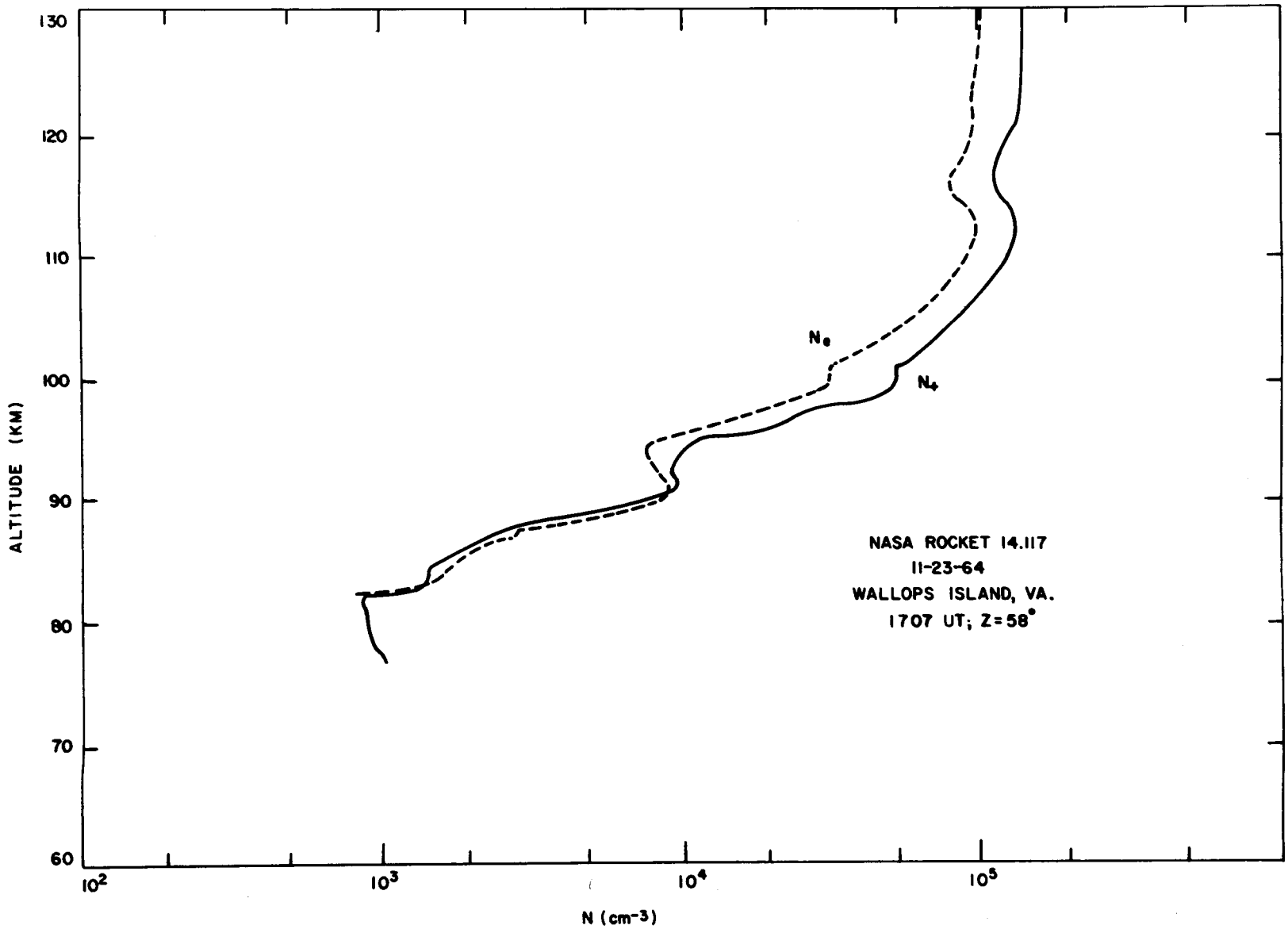

Figure 2. Rocket measurement of (a) positive ion density, N_+ as represented by solid curve, (b) electron density, N_e, as represented by dashed curve.

ment within experimental error at altitudes between 85 and 90 km. Below 80 km, the electron density falls somewhat below the limiting sensitivity of the radio-propagation experiment which is about $10^3 cm^{-3}$, suggesting that $N_+ > N_e$ and thus that negative ions may be important throughout the D region. Above 90 km, the N_+ values are apparently higher by an average of 25 percent. The difference is, of course, not real. The N_e values agree with a ground-based ionosonde which was operative throughout the launch. There are two possibilities for explaining the apparently high N_+ values above 90 km. Firstly, an automatic sensitivity change in the electrometer associated with the ion density experiment took place just below 90 km. It is possible that the discrepancy above 90 km reflects a miscalibration of this sensitivity range of the electrometer. Secondly, it is possible that above 90 km the vehicle potential becomes sufficiently negative so that the effective ion collection area is slightly larger than the physical aperture area used in equation (1) to compute N_+. However, a previous rocket flight of an analogous set of experiments (Bauer et al, 1964) did not show this large a difference. An electrometer miscalibration also is favored because on the other Nike-Apache launch discussed here results from an identical ion density experiment were in exact agreement with an ionosonde determination of f_oE.

In any event, the 25 percent apparent and constant difference above 90 km shown in Figure 2 is not at all crucial to our subsequent interpretation of these data in terms of processes which govern the formation of the lower ionosphere. We emphasize that the two curves are identical in shape above 85 km and that each was taken with an extremely fine altitude resolution (approximately 10 meters for the N_+

experiment). This resolution is important since in subsequent sections it permits us to show that (a) the change in slope at about 88 km marks the transition from ionization by 2-8Å X-radiation to ionization by the C VI line at 33.7Å, (b) the large discontinuity at 90-95 km in an otherwise monotonically increasing density curve is due partially to transition from ionization by the C VI line to ionization by Lyman β (1025.7Å) but, more importantly, it also results from a change in the effective ion-electron recombination rate, (c) the small discontinuity at 100-102 km occurs where production due to 40-75Å X-radiation is a maximum and (d) the minimum at 115 km reflects the transition from ionization due to Lyman β to ionization by radiation in the 80-977Å region.

To arrive at these interpretations we must know (a) the characteristics of the neutral atmosphere, (b) the absorption and photoionization cross sections of the individual neutral constituents as a function of solar radiation wavelength (λ), (c) the intensity of solar radiation measured above the atmosphere as a function of λ and (d) chemical reaction rates. In the next two sections, we show that for the most part parameters (a) and (c) were measured during the rocket flight leaving us with the ability to suggest the nature of the chemical reactions as well as their approximate rates.

MEASUREMENT OF OPTICAL DEPTH

To date, one of the principal uncertainties in computing photoionization rates in the ionosphere has been in our knowledge of neutral gas parameters, specifically the density, temperature and the total absorption cross sections of the individual constituents. All of these parameters are embodied in the optical depth, τ, which is given by

$$\tau = \sum_j H_j \, n_j \, \sigma_{j\lambda} \, \sec Z \qquad (2)$$

where j denotes the absorbing constituent, H, n and σ its scale height, density and absorption cross section, respectively, and Z is the solar zenith angle.

On one of the two rocket flights discussed here, we have measured τ for λ = 1215.7Å (Lyman alpha) with an error of less than 20 percent by use of a photoelectron retarding potential analyzer experiment modeled after Hinteregger et al (1959). Our experiment shown pictorially in Fig. 1 is a series of concentrically-arranged planar electrodes. The aperture and second grids were biased to exclude ionospheric electrons and positive ions, respectively. The potential of the third grid was varied in a manner designed to measure the energy of electrons emitted from the tungsten target as the spinning rocket periodically exposed the sensor to solar radiation.

The spectral response of a tungsten target as compiled by Whipple (1965) is presented in Figure 3 together with references to the laboratory investigations from which the curve was derived. This curve together with the knowledge that the intensity of extreme ultraviolet (EUV) radiation far exceeds that of X-radiation leads to the conclusion that the experiment practically responds only to EUV for zero photoelectron retardation potential.

The measured photocurrent emitted from a tungsten target of area 10 cm^2 when at zero retarding potential is plotted as a function of altitude in Figure 4. The rocket was flown for a solar zenith angle of 58^o. The large increase observed between 60 and 90 km clearly identifies the region where Lyman alpha radiation is absorbed. The increase from 150 km to the apogee altitude of 182 km is attributable to decreasing absorption of the spectral region 170-796Å which ionizes the F region. An extrapolation of this curve above rocket

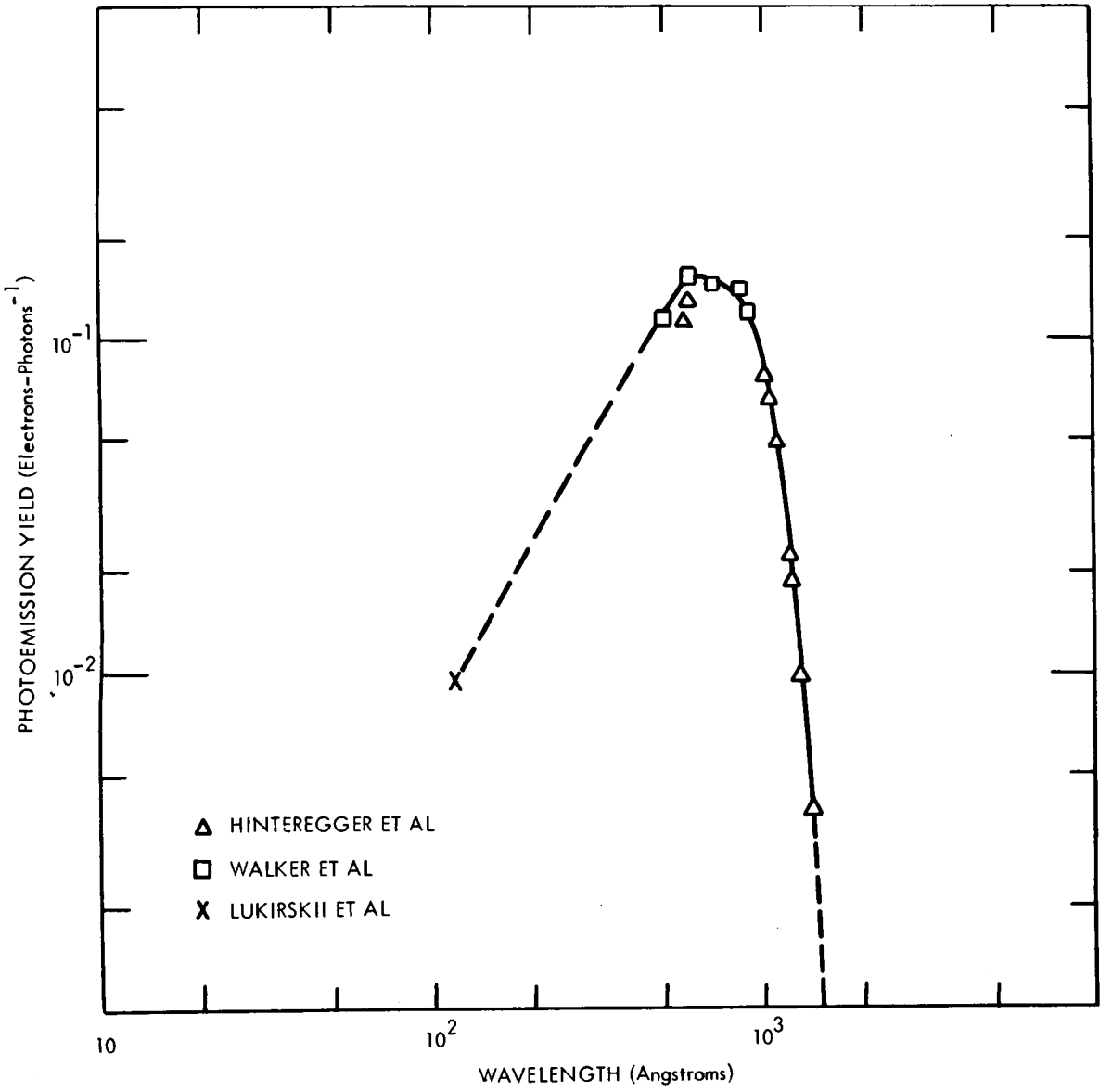

Figure 3. Photoelectric yield of tungsten as a function of wavelength.

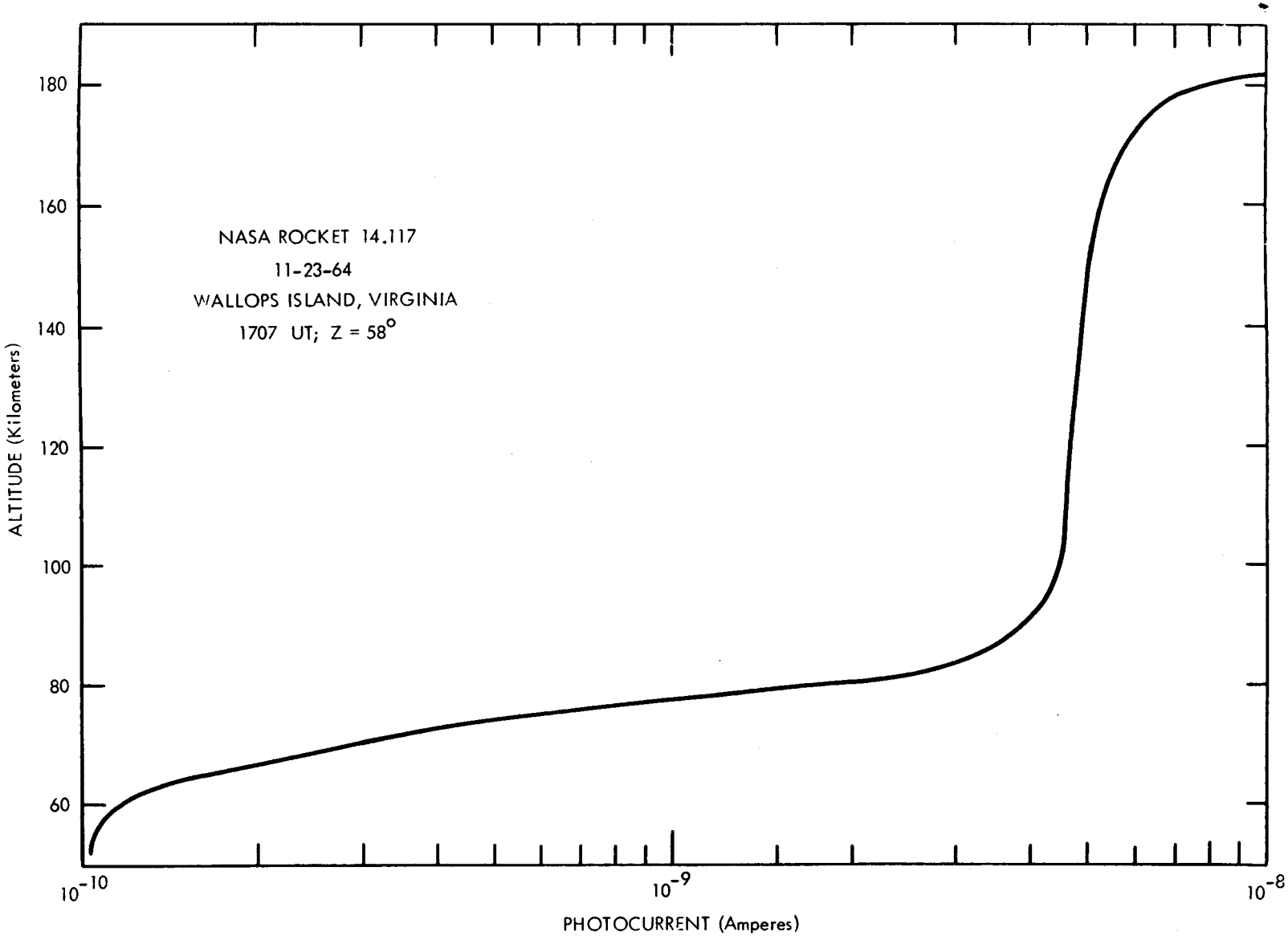

Figure 4. Rocket measurement of unretarded photocurrent from a tungsten target.

apogee would lead to a photocurrent density consistent with the value of 5×10^{-9} amps cm^{-2} measured well above the atmosphere on the Explorer 8 satellite (Bourdeau et al, 1961).

The data from Figure 4 can be used to obtain the optical depth because the ratio of the current at a given altitude ($I_{z\lambda}$) to its value above the atmosphere ($I_{o\lambda}$) is given by $e^{-\tau}$. The circled points in Figure 5 represent rocket values of the ratio $I_{z\lambda}/I_{o\lambda}$ obtained by normalizing all the measured points for zero retardation to the value observed at 120 km. This essentially provides a measure of $e^{-\tau}$ for Lyman alpha radiation. The solid curve in Figure 5 is $e^{-\tau}$ computed from equation 2 by setting $Z = 58^{o}$, using the 1962 US Standard Atmosphere and a value for σ_{o_2} of $10^{-20} cm^2$ as measured for the Lyman alpha line by Watanabe (1954). Except for the region below 75 km, the agreement between the experimental points and the computed curve is better than 20 percent. This, then, is about the level of confidence which can be placed on our choice of a reference neutral atmosphere and of σ_{o_2} for $\lambda = 1215.7\text{Å}$. The excess measured current below 75 km is attributable to photocurrent produced by the 2100 to 3000Å portion of the solar spectrum.

The resolution of our experiment on this particular flight is insufficient for us to determine the optical depth corresponding to other EUV lines important to our study here. For example, even though from Figure 3 the photoemission yield efficiency for Lyman β (1025.7Å) is four times that of Lyman alpha, the latter radiation is approximately two orders of magnitude more intense, leaving us with a search for a 4 percent effect. Our volt-ampere curves do show an expected hardening of the photoelectron spectrum above the accepted absorbing region for Lyman β (100-120 km). On future flights, we hope to separate out these other wavelengths by

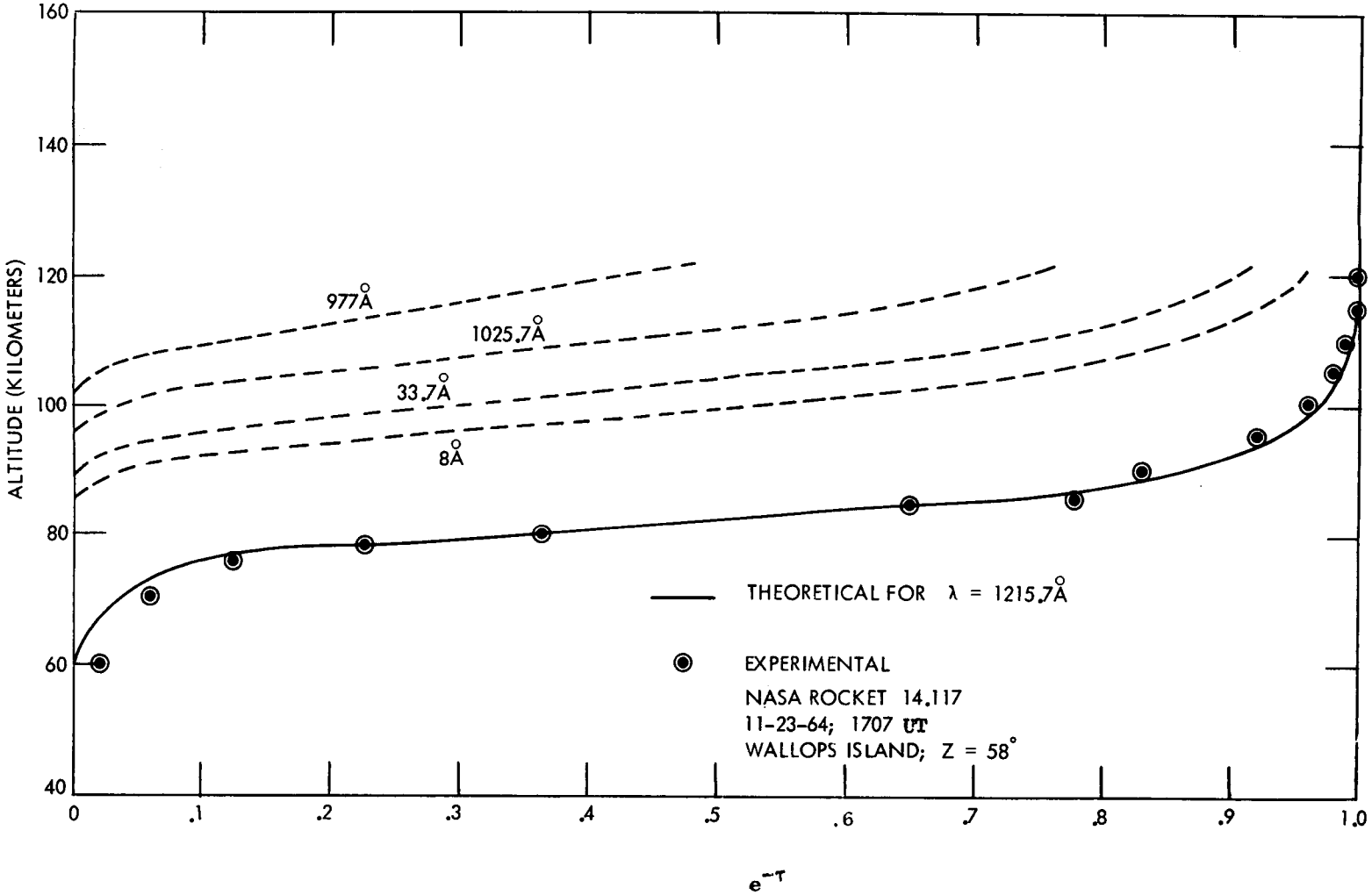

Figure 5. The effect of attenuation by the terrestrial atmosphere for specified wavelengths including an experimental and theoretical comparison for the Lyman alpha line.

appropriate choice of fixed photoelectron retarding potentials.

PRODUCTION RATES

The solar radiation wavelengths of primary importance to our study are 1215.7Å, 2-8Å, 33.7Å, 977-1025.7Å and 40-75Å. The altitude of maximum electron production (q_m) for a specific wavelength is approximately that of unit optical depth, for which $e^{-\tau} \cong 0.37$. The solid curve in Figure 5 shows that this occurs at approximately 80 km for the measured transmission of Lyman alpha radiation where $Z = 58^o$. The altitudes of q_m for $Z = 58^o$ and for other spectral lines can be deduced from the dashed curves in Figure 5.

The photoionization rate at a given altitude is given by

$$q = \sum_{\lambda} \sum_{j} \sigma'_j \; n_j \; k_{\lambda j} \; \Phi_{o\lambda} \; e^{-\tau} \qquad (3)$$

where k is the number of ion pairs produced per photon, $\Phi_{o\lambda}$ is the number of incident photons of wavelength λ at the top of the atmosphere, and σ'_j is the ionization cross section of the j^{th} constituent. The absorption cross sections which will be used here for calculating q were taken from Watanabe and Hinteregger (1962), Nicolet (1961), and Samson and Cairns (1964). Values for k were taken from Norton et al (1963) and Nicolet and Aikin (1960).

The spectral lines or regions in Table I are grouped to reflect increasing altitudes of influence. The listed fluxes for the EUV, the 95Å and the 140Å emissions are taken from Watanabe and Hinteregger (1962) after taking into account the solar cycle variation indicated by Hall et al (1965), the change with solar cycle being relatively small for the EUV radiation. Measurements made at the time of our rocket flights with the aid of the NRL Radiation Monitoring Satellite

(Kreplin, private communication) show the radiation intensity in the spectral range 0-8Å was less than 2.5×10^{-4} ergs $cm^{-2} sec^{-1}$.

TABLE 1. Solar Radiation Intensity and Altitude of Unit Optical Depth as a Function of Wavelength.

λ	$\Phi_{o\lambda}$	$z(\tau = 1; Z = 58^{o})$
Å	$ph.cm^{-2} sec^{-1}$	km
2	1.00×10^{0}	72
1215.7	2.70×10^{11}	80
4	2.00×10^{2}	83
6	1.20×10^{4}	90
8	1.00×10^{5}	95
33.7	7.63×10^{6}	100.0
989.8-1025.7	3.50×10^{9}*	108.0**
40-75	7.50×10^{7}*	112.0**
977	3.00×10^{9}	115.0
95	2.50×10^{8}	125.0
140	3.50×10^{8}	130.0

*Total intensity integrated over the indicated spectral region.
**Mean altitude for the indicated spectral region.

The tabulated fluxes for this range represent upper limits estimated by W. White (private communication) from the prevailing 10.7 cm radio flux and Ca plage activity.

The absorption cross sections for λ = 8-31Å are equivalent to those for λ = 31-90Å (Nicolet and Aikin, 1960). Thus these two radiation bands ionize the same ionospheric regions. However, the radiation for λ = 8-31Å is, in general, more than one order of magnitude less intense, thus making these wavelengths unimportant to our study.

Our production rate calculations have made use of the recent availability of identified spectral lines in the 33.7-72.3Å observed by Tousey et al (1963). These photographs of the solar spectrum have been converted to the relative intensities of the various lines (Widing, private communication). This has enhanced our ability to assess the role which this very important spectral range plays in the formation of the lower E region. In our electron production rate calculations, the relative line intensities were normalized to the integrated flux values for λ = 44-60Å measured with the NRL Satellite at the time of the rocket launches. Production rates for some 23 identified lines were computed individually and then summed to obtain a total effect for λ = 40 to 75Å. The C VI line at 33.7Å was considered separately because its importance to E region ionization at solar minimum exceeds that of the other 23 combined.

As indicated in the previous section, the N_2 and O_2 densities which we use for production rate calculations below 100 km are based on the results of the photoelectron retarding potential experiment. They are consistent with what would be obtained by use of the US Standard Atmosphere for total density and assuming mixing to derive the density of the individual constituents. Above 100 km, we used the amount of dissociation of the molecular constituents indicated by Nicolet (1963) normalized to total density from the US Standard Atmosphere. The relative O, O_2, N_2 abundances used

agree with mass spectrometric measurements (Nier et al, 1964) well enough for our application.

The results of our production rate calculation corresponding to the rocket flight where $\chi = 58^{o}$ are presented in Figure 6. Each curve represents the sum of O_2^+ and N_2^+ production. Not included but reserved for subsequent discussion is the production of NO^+ due to Lyman alpha radiation. It is seen from the solid curves that (a) radiation at 2-8Å is mainly responsible for ionizing the region 82-90 km, (b) the C VI line at 33.7Å first identified by the NRL group is the principal ionization source at 90-95 km and (c) that the altitude interval 95-115 km is dominated by the 977-1025.7Å band. It should be noted from the dotted curve, however, that X-radiation at 40-75Å is important to the 95-120 km region and from the dashed curves that 85-170Å X-radiation is important to ionization of the region above 120 km.

In summary we conclude for our ionospheric conditions that at solar minimum as the altitude is increased up to 120 km, the ionosphere is successively produced mainly by Lyman alpha, 2-8Å, 33.7Å, and 977=1025.7Å radiation. This conclusion is apt to change, however, for other than solar minimum conditions and/or flare activity when the X-radiation intensity relation to the EUV flux can be expected to increase.

EFFECTIVE RECOMBINATION COEFFICIENTS (83-120 KM)

A complete model for the formation of any ionospheric subdivision must take into account loss mechanisms as well as production phenomena and the net charged particle density. Under equilibrium conditions and above 83 km (where $N_+ = N_e$), production and loss can be related to the charged particle density by

$$q = \alpha_{ie} N_e^2 \qquad (4)$$

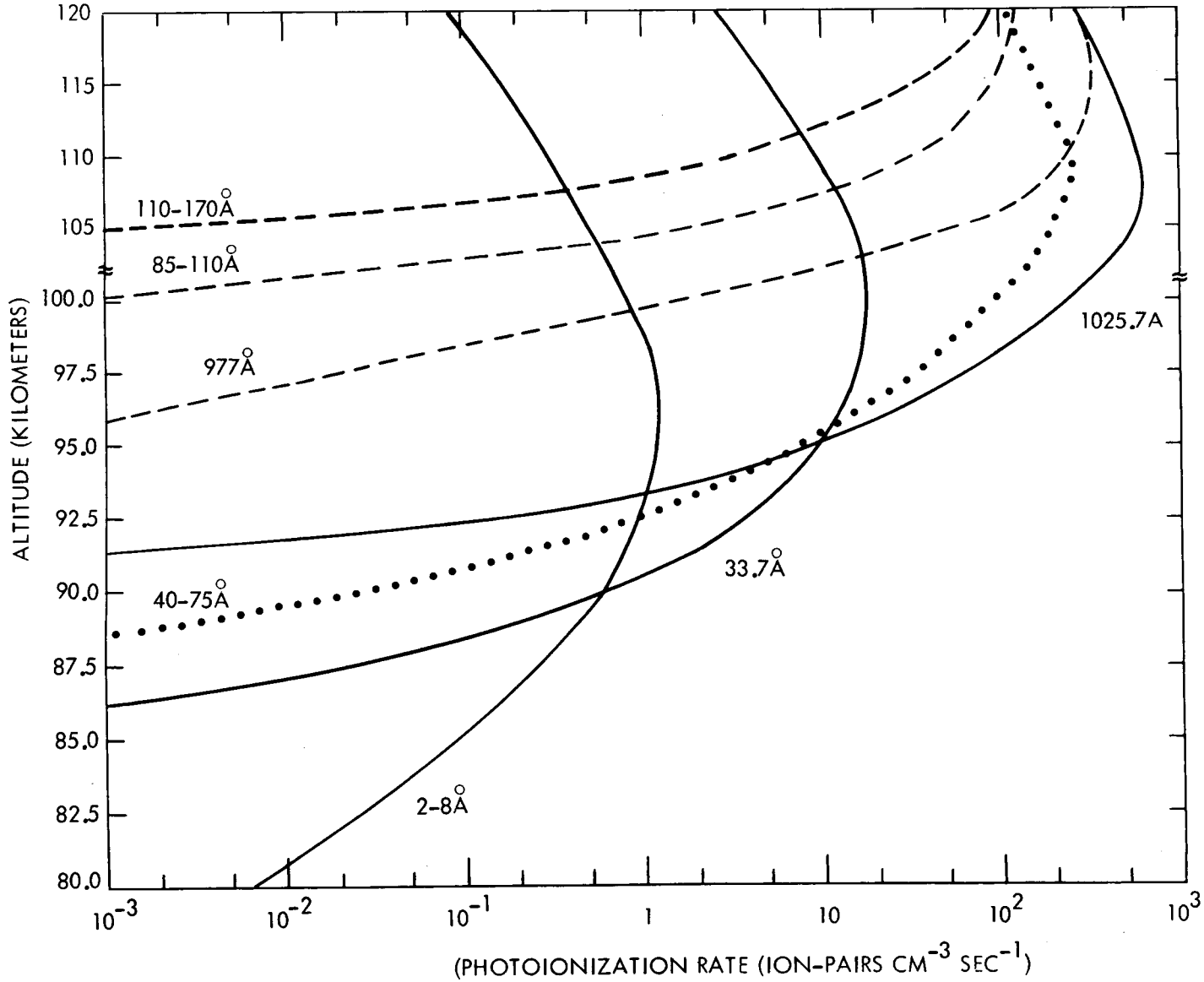

Figure 6. Total photoionization rate as a function of altitude for specified wavelengths and wavelength bands.

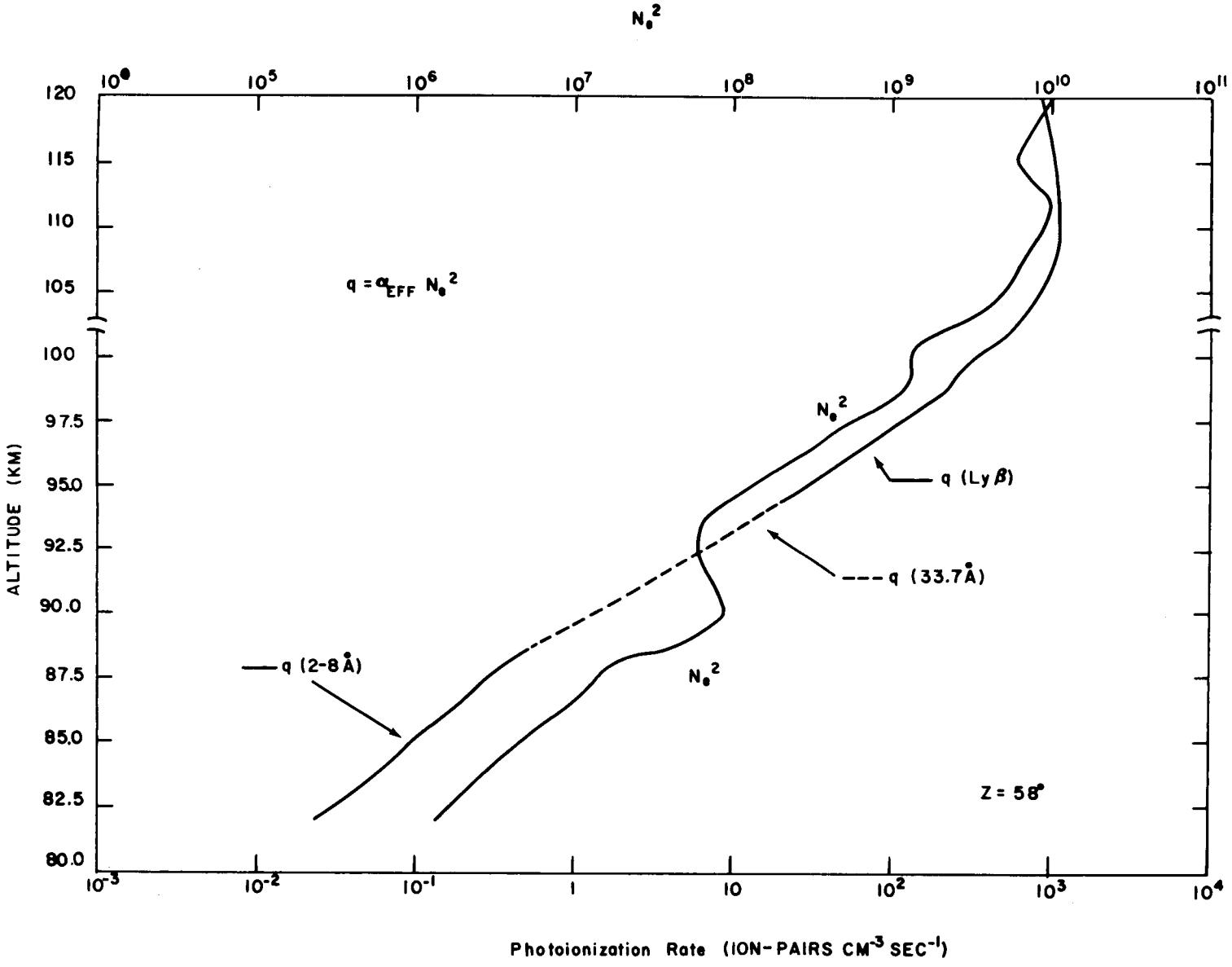

Figure 7. Total ion pair production function and N_+^2 plotted as a function of altitude for $Z = 58^o$ rocket experiment.

where α_{ie} is the effective rate for ion-electron dissociative recombination. Equation (4) is valid only if ion-electron dissociative recombination is the dominant charged particle loss mechanism and if chemical processes are more important than charge transport. To develop our model, we have plotted in Fig. 7 the square of the measured charged particle densities together with the total production rate q_t derived by summing the effects of the individual spectral lines and regions shown in Figure 6.

The region (82-88 km) where 2-8Å radiation is the dominant source of ionization is identified as the solid portion of the q_t curve. This conclusion is supported by the parallelism between the q_t and N_e^2 in this altitude interval. For this region we compute α_{ie} to be $2 \times 10^{-8} cm^3 sec^{-1}$. We emphasize that this is probably an upper limit for α_{ie} since we also have used an upper limit for the intensity of the 2-8Å radiation.

The dashed portion of the q_t curve identifies the region where 33.7Å radiation is predominant. We note that at about 88 km there is a change in the slope of q_t accompanied by a corresponding but more pronounced change in the slope of N_e^2. This corresponds to the altitude where according to Figure 6, 33.7Å X-radiation is becoming important. In the region 88-90 km the computed value of α_{ie} is within a factor of two of that computed for the 82-88 km region.

Most importantly, we note that in the region 90-93 km the relative positions of the q_t and N_+^2 curves <u>reverse</u>. We interpret this as indirectly due to a change from production by X-radiation to production by EUV but directly associated with a change in the effective dissociative recombination coefficient, α_{ie}.

Finally, we note that from 93 to 105 km, the N_+^2 curve tracks the q_t curve quite well. This is the altitude region where from Figure 6 we suggest that Lyman β is the predominant source of ionization. The computed value for α_{ie} in this region is approximately $1.8 \times 10^{-7} cm^3 sec^{-1}$, suggesting that the charged particles are lost at about ten times the rate computed for the region produced by X-radiation. The inflection point in both the q_t and N_+^2 curves at exactly 100 km probably reflects the peak in the production by 40-75Å X-radiation together with the emergence of the EUV C III line at 977Å (see Fig. 6).

Our other rocket flight occurred for $Z = 25^o$. Unfortunately, the radio-propagation experiment designed to measure N_e malfunctioned on this flight. However, successful ion density results were obtained and are compared with the other N_+ profile in Fig. 8. The smaller values throughout the altitude region below 105 km for $Z = 58^o$ are entirely attributable to the higher solar zenith angle. So too are the greater number of discontinuities in the profile for $Z = 58^o$. We suggest that the separation of regions ionized by different parts of the solar spectrum is much more distinct for large solar zenith angles than for an overhead sun if the EUV and X-ray fluxes are in the right proportion.

Our comparison of the computed production rate with N_+^2 for $Z = 25^o$ are with one exception consistent with those shown in Fig. 7 for $Z = 58^o$. We obtain the same values for α_{ie} of about 1.8×10^{-7} and $2 \times 10^{-8} cm^3 sec^{-1}$ for the regions ionized by Lyman β and 33.7Å X-radiation respectively. The one exception is in the region produced by 2-8Å X-radiation where either lower values of q or higher values of α_{ie} are indicated. Of these two possibilities, we favor a lower production rate from the following arguments.

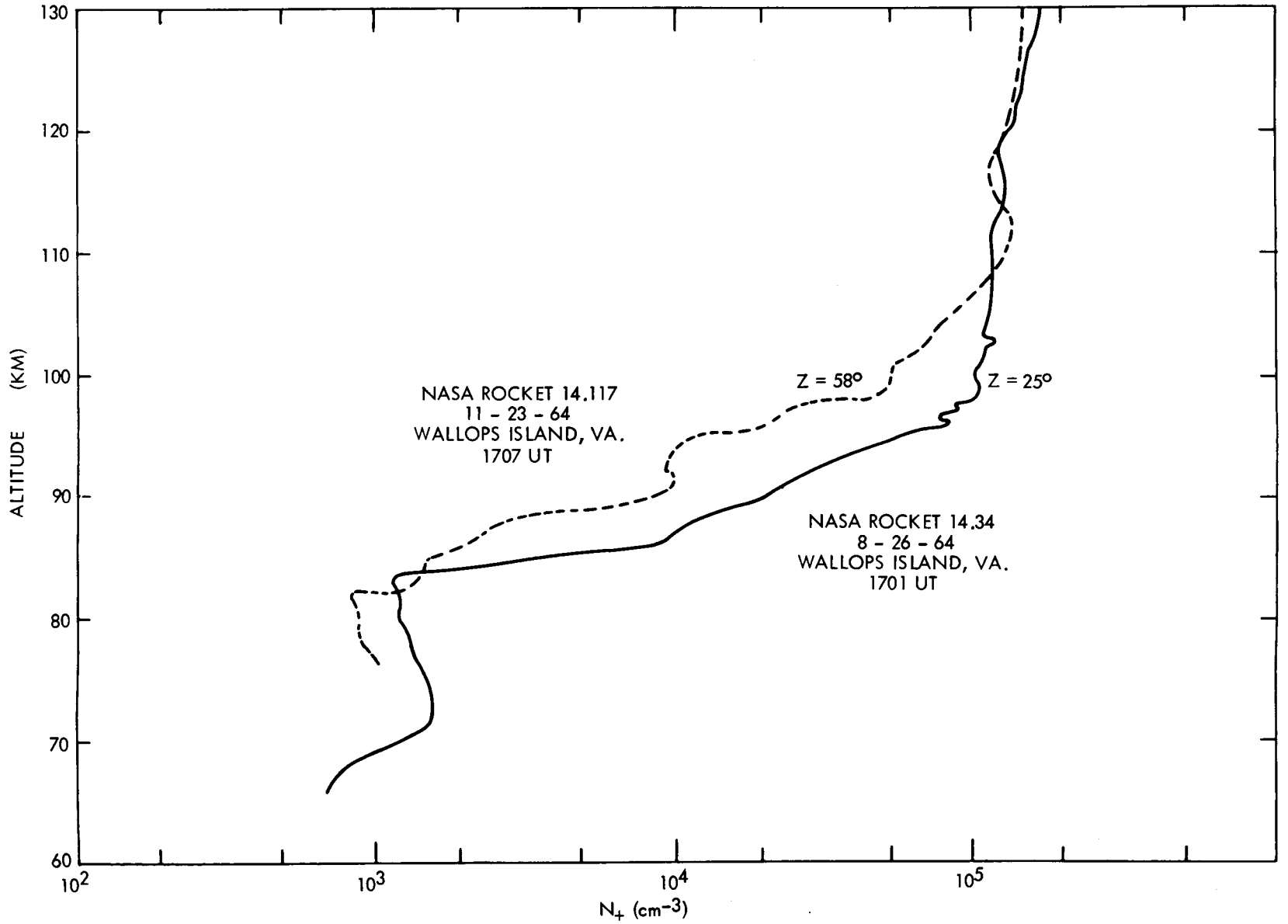

Figure 8. Comparison of positive ion density as measured by two rockets launched at two different solar zenith angles.

From the NRL satellite observations we know only the upper limit for the intensity of the 2-8Å radiation in both cases. Our comparison of q and N_+^2 suggest that this intensity was lower on 26 August than on 23 November 1964. This is consistent with observations from the NRL satellite in the 44-60Å region which suggest that the minimum in solar X-radiation was reached in July-August, 1964.

From our results it may be concluded that (a) EUV can be the predominant source of ionization in the lower E region during periods of low solar activity and (b) there is a drastic change in the value of α_{ie} below 90 km where X-radiation dominates and the value above 90 km where EUV is more important. Below 115 km,

$$\alpha_{ie} = \frac{\alpha_1 n_1 + 2 n_2}{n_1 + n_2}, \tag{5}$$

where the subscripts (1) and (2) denote NO^+ and O_2^+, respectively. An altitude-dependent α_{ie} such as we observe implies that the ratio $n_{O_2^+}/n_{NO^+}$ is a function of altitude and that α_{NO^+} and $\alpha_{O_2^+}$ differ from one another. The consistency of these conclusions with recent ion mass spectrometer results and with measurements of ion-neutral reaction rate coefficients is examined in the next section.

IONIC REACTIONS

Consider first the region below 90 km where N_2^+ and O_2^+ are produced by X-radiation. The rate γ_1, for the process

$$N_2^+ + O_2 \rightarrow O_2^+ + N_2 \tag{6}$$

is between 1 and $2 \times 10^{-10} cm^3 sec^{-1}$ (Feshenfeld, et al, 1965b; Fite et al, 1962). For rates of this magnitude N_2^+ will be removed by process (6) rather than by either dissociative recombination or by ion-atom interchange. Thus, both as a consequence of (6) as well as direct photoionization of O_2, the problem below 90 km is reduced to a method for removing O_2^+ ions. There are two possibilities, ion-atom interchange,

$$O_2^+ + N_2 \rightarrow NO^+ + NO \qquad (7)$$

which has a rate γ_2 less than $10^{-15} cm^3 sec^{-1}$ (Ferguson, private communication) and dissociative recombination

$$O_2^+ + e \rightarrow O + O \qquad (8)$$

for which $\alpha_{O_2^+}$ is about $2 \times 10^{-7} cm^3 sec^{-1}$ (Biondi, 1964). Process (7) will prevail over (8) if $\gamma_2 n_{N_2}$ exceeds $2 \times 10^{-7} N_e$. By using the 1962 US Standard Atmosphere for n_{N_2} and our measured value for N_e, we find that this will occur below 90 km if $\gamma_2 > 2 \times 10^{-17} cm^3 sec^{-1}$. For this case, the positive ion species below 90 km will be almost entirely NO^+. The origin of this ion is the photoionization of O_2 followed by process (7) combined with photoionization of N_2 followed by a two-step process given sequentially by (6) and (7). Recent ion spectrometer observations (Johnson, private communication; Narcisi and Bailey, 1965) confirm that NO^+ is the dominant ion below 90 km. Thus, our value for α_{ie} of $2 \times 10^{-8} cm^3 sec^{-1}$ below 90 km quite likely represents α_{NO^+}. If so, our value is in agreement with some other ionospheric measurements (Holmes et al, 1964) but an order of magnitude less than laboratory measurements (Doering and Mahan, 1962).

Because of the increase in the O/O_2 ratio, the ionic chemistry of the altitude region 95-115 km is even more

complicated. Our computations show that below 115 km photoionization of atomic oxygen has little effect on the total production rate. According to rates published by Feshenfeld et al (1965a,c) the rate for conversion of O^+ ions through

$$O^+ + O_2 \rightarrow O_2^+ + O \qquad (9)$$

is much greater than that of

$$O^+ + N_2 \rightarrow NO^+ + N \qquad (10)$$

As a result, between 95 and 115 km where O_2 dissociation is relatively small, photoionization of O will contribute to the O_2^+ density. This will be a small contribution because of the low O^+ production rates at these altitudes.

If γ_2 is less than $10^{-15} cm^3 sec^{-1}$ as indicated by Ferguson (1965) dissociative recombination is more important than ion-atom interchange (7) for removing O_2^+. Consequently, our computed value for α_{ie} of $1.8 \times 10^{-7} cm^3 sec^{-1}$ between 95 and 115 km partially reflects $\alpha_{O_2^+}$.

Since (10) is negligible compared to (9), and since (7) is small compared to (8), NO^+ ions between 95 and 115 km are an indirect result of photoionization of N_2. Ferguson et al (1965) have deduced from laboratory measurements a rate of $2.5 \times 10^{-10} cm^3 sec^{-1}$ for the process

$$N_2^+ + O \rightarrow NO^+ + N, \qquad (11)$$

a reaction first considered important in the ionosphere by Norton et al (1963). Such a large rate coefficient can lead to equal concentrations of O_2^+ and NO^+ in the 95 to 115 km region even though N_2 production resulting from 40-75A

radiation is less than O_2^+ production by EUV radiation. The exact ratio of O_2^+ and NO^+ critically depends on the O/O_2 ratio. Ion spectrometer observations (Narcissi and Bailey, 1964; Holmes et al, 1964) show O_2^+ and NO^+ to be of equivalent importance at 100 km during periods of low solar activity. If so and if the value for α_{NO^+} of $2 \times 10^{-8} cm^3 sec^{-1}$, which we derived for the region below 90 km, can be applied here, then a value of about $3.6 \times 10^{-7} cm^3 sec^{-1}$ would be inferred for $\alpha_{O_2^+}$ by use of eq. 5.

THE D REGION AT SOLAR MINIMUM

The interpretation of our results in the D region requires firstly a discussion of the average value of N_+ measured by us below 83 km. The lowest altitude at which we can make N_+ measurements is governed by the altitude of nose cone ejection. Since this occurred as low as 66 km for $Z = 25^o$ our discussion will emphasize this flight. The average value of N_+ observed in the D region by our experiment is a little more than $10^3 cm^{-3}$. This is an order of magnitude less than the results reported by other investigators who used exposed probes. As we emphasized in a previous section our experiment has the advantages of relative insensitivity to unwanted photocurrent, to vehicle potential and does not require a detailed knowledge of other ionic parameters to derive N_+. As to possible effects due to shock waves generated by the passage of a supersonic vehicle through this region of high pressure, we note very good agreement between our N_+ values and those since obtained by L. G. Hale (private communication) who used an entirely different device set to subsonic velocities by use of a parachute.

In Fig. 9 we have plotted N_+^2 as a function of altitude in the region 65-90 km for the rocket flight where $Z = 25^o$. For comparison, we additionally present a suggested positive

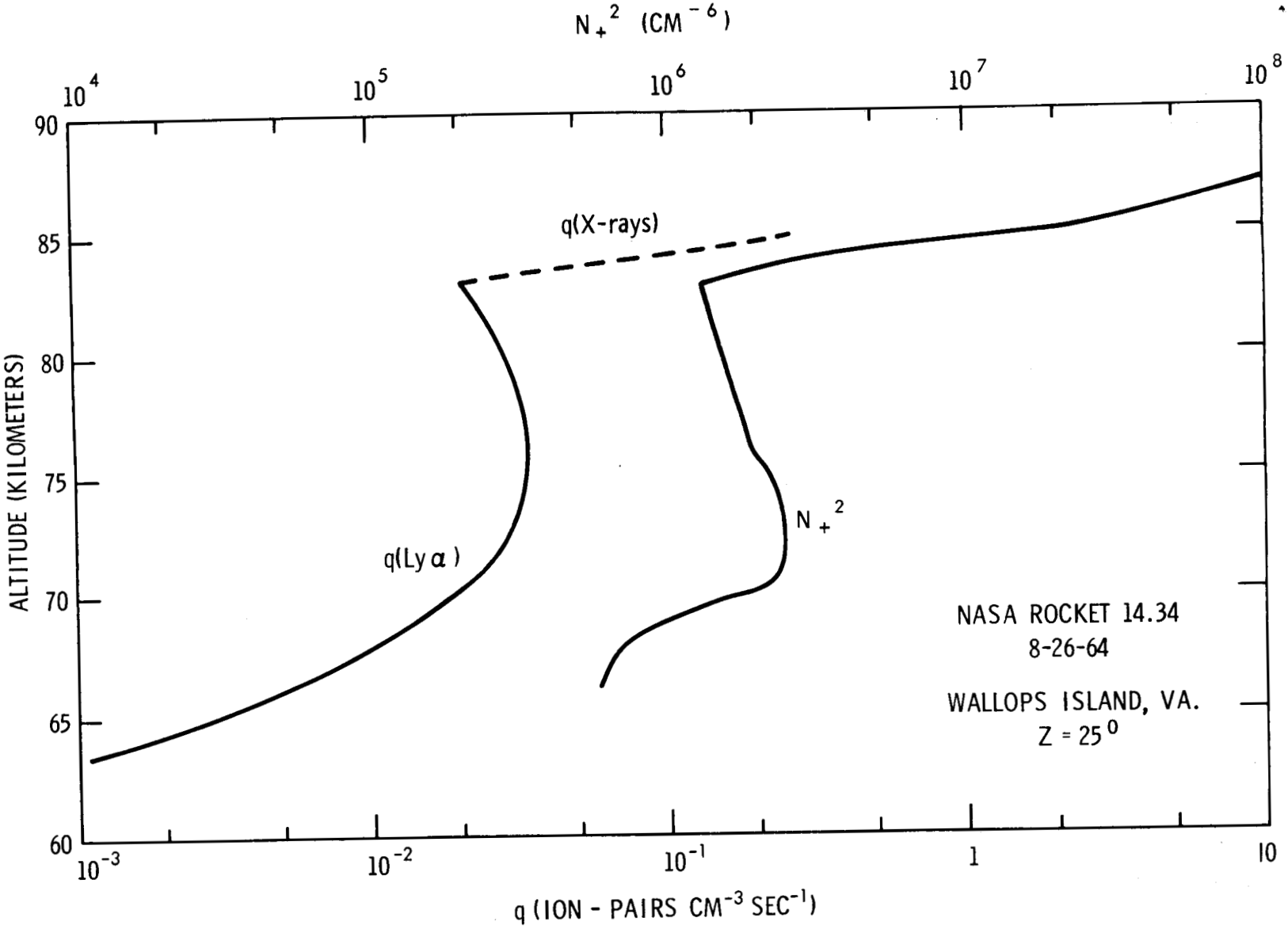

Figure 9. Comparison of the square of the positive ion density with the ion pair production function for the D region.

ion production rate for this altitude interval. The upper portion of the q curve is due to X-radiation and was discussed in previous sections. We emphasize that for this portion of the curve we are reasonably confident of the density of the ionizable constituents and that we have a measure of at least the upper limit for the intensity of X-radiation. We consequently have some confidence that at the altitude (83 km) separating the D and E region the production rate is approximately 2×10^{-2} ion pairs $cm^{-3}sec^{-1}$. Unless one is willing to accept a drastic change in the effective loss rate at this altitude, this value for q permits us to normalize on an absolute basis the production rate due to the Lyman α radiation responsible for ionizing the D region. The values for q which were computed for the region below 83 km (Fig. 9) consequently are consistent with a density of the trace ionizable constituent, nitric oxide, given by

$$n_{NO} \cong 3 \times 10^{-10} \, n_{O_2} \qquad (12)$$

Aikin et al (1964) point out that one can from laboratory and rocket observations obtain three very different models of the n_{NO} distribution. The one given by Eq. 12 which is based on our rocket results gives an NO abundance consistent with curve 1 of their paper and their derived effective recombination coefficient at 80 km.

In the D region, we must allow for the possible existence of negative ions. For equilibrium conditions

$$q = \alpha_{ie} N_+ N_e + \alpha_{ii} N_+ N_- \qquad (13)$$

where α_{ii} is the ion-ion recombination coefficient. The effective loss rate for positive ions computed throughout

the D region from Fig. 9 varies from 1.2 to 2 x 10^{-8} cm^3 sec^{-1}. The absence of a simultaneous and accurate electron density measurement prevents us from inferring with confidence the nature of this loss mechanism. If negative ions are unimportant, then ion-electron recombination dominates and we have a value for α_{NO^+} consistent with that deduced at higher altitudes where X-radiation is the dominant source of ionization. However, even our low values of N_+ are higher than N_e values obtained under similar ionospheric conditions on other rockets (Aikin et al, 1964). Thus, there is a probability that negative ions are important throughout the D region and that positive ions are removed by ion-ion recombination. Fortuitously for this case, $\alpha_{ii} \cong \alpha_{NO^+} \cong 2 \times 10^{-8} cm^3 sec^{-1}$. This cannot be a firm conclusion, however, until N_+ and N_e are simultaneously and accurately measured throughout the D region.

CONCLUSIONS

From our rocket measurements of charged particle density and optical depth together with simultaneous satellite observations of solar radiation flux, we suggest that the following production and loss mechanisms prevail during the year of the minimum solar activity:

At altitudes between 65 and 83 km, the important ionization source is Lyman alpha radiation acting on the trace constituent nitric oxide whose abundance is approximately given by 3 x 10^{-10} n_{O_2}. The effective loss rate for positive ions in this region is approximately 2 x 10^{-8} cm^3 sec^{-1}.

The region 82-88 and 88-93 km is successively produced by 2-8 Å and 33.7 Å X-radiation. On the assumption that the ion-atom interchange, $O_2^+ + N_2 \rightarrow NO^+ + NO$, takes place at

a rate faster than 2 x 10^{-17} $cm^3 sec^{-1}$ the principal ionic species in this region is NO^+. As a consequence, the computed effective loss rate of 2 x 10^{-8} $cm^3 sec^{-1}$ represents dissociative recombination of NO^+ ions with electrons.

The region 93-115 km is ionized principally by EUV radiation producing mainly O_2^+ and by 40-75Å radiation producing mainly N_2^+. The N_2^+ ions are removed by charge transfer with atomic oxygen and/or ion interchange with O_2 leading to a region where NO^+ and O_2^+ ions are of equivalent importance. The effective recombination rate in this region is about 1.8 x 10^{-7} $cm^3 sec^{-1}$ with $\alpha_{O_2^+}$ estimated to be about twice that value.

Care must be taken not to extend these conclusions to other levels of solar activity. Our analysis of the formation of the lower ionosphere for this case is consistent with all laboratory measurements of the pertinent reactions except α_{NO^+}.

ACKNOWLEDGMENTS

The rocket payloads were instrumented under the direction of G. Spaid and R. Hagemeyer. The electron density profile in Fig. 2 was derived by J. E. Jackson and S. J. Bauer. We are grateful to R. Kreplin and K. Widing of the Naval Research Laboratory for their solar radiation data and to C. Y. Johnson for access to spectrometer observations below 120 km. Discussions with our Goddard colleagues, S. J. Bauer and W. White are gratefully acknowledged.

REFERENCES

Aikin, A. C., Jr., J. A. Kane and J. Troim, J. Geophys. Res., 64, 4621, 1964.

Bauer, S. J., L. J. Blumle, J. L. Donley, R. J. Fitzenreiter and J. E. Jackson, J. Geophys. Res., 69, 186, 1964.

Biondi, M. A., Ann. de Geophysique, 20, 34, 1964.

Bourdeau, R. E., J. L. Donley, G. P. Serbu and E. C. Whipple, Jr., J. Astron. Sci., 8, 65, 1961.

Bourdeau, R. E., E. C. Whipple, Jr., and J. F. Clark, J. Geophys. Res., 64, 1363, 1959.

Doering, J. P. and B. H. Mahan, J. Chem. Phys., 36, 669, 1962.

Fehsenfeld, F. C., A. L. Schmeltekopf and E. E. Ferguson, Planetary Space Sci., 13, 219, 1965a.

Fehsenfeld, F. C., A. L. Schmeltekopf and E. E. Ferguson, Planetary Space Sci., in press, 1965b.

Fehsenfeld, F. C., P. D. Goldan, A. L. Schmeltekopf and E. E. Ferguson, Planetary Space Sci., in press, 1965c.

Ferguson, E. E., F. C. Fehsenfeld, P. D. Goldan, A. S. Schmeltekopf and H. I. Schiff, Planet. Space Sci. (in press).

Fite, W. L., J. A. Rutherford, W. R. Snow and V. A. Van Lint, Disc. Far. Soc., 33, 264, 1962.

Hall, L. A., W. S. Schweizer and H. E. Hinteregger, J. Geophys. Res., 70, 2241, 1965.

Hinteregger, H. E., K. R. Damon and L. A. Hall, J. Geophys. Res., 64, 1961, 1965.

Holmes, J. C., C. Y. Johnson and J. M. Young, Space Research V, to be published, Florence, Italy, 1964.

Lukirskii, A. P., M. A. Rumsh and L. A. Smirnov, Optics and Spectros., 9, 265, 1960.

Narcisi, R. S. and A. D. Bailey, Air Force Cambridge Research Laboratories Report 65-81, 1965.

Nicolet, M., Aeronomy, to be published in Handbook der Physik, Prepublication Copy, 1961.

Nicolet, M., Ionosphere Research Laboratory Report 183, Penn. State Univ., 1963.

Nicolet, M. and A. C. Aikin, Jr., J. Geophys. Res., 65, 1469, 1960.

Nier, A. O. J. H. Hoffman, C. Y. Johnson and J. C. Holmes, J. Geophys. Res., 69, 4629, 1964.

Norton, R. B., T. E. Van Zandt and J. S. Denison, Proceedings of the International Conference on the Ionosphere, Bartholomew Press, 26, 1963.

Samson, J. O. and R. B. Cairns, J. Geophys. Res., 69, 4583, 1964.

Tousey et al, Report of AAU, Wash., 1963, reported in Sky and Telescope, 1964.

Walker, W. C., N. Wainfan and L. Weissler, J. Appl. Phys., 26, 1366, 1955.

Watanabe, K., J. Chem. Phys., 22, 1564, 1954.

Watanabe, K. and H. E. Hinteregger, J. Geophys. Res., 67, 999, 1962.

Whipple, E. C., Jr., Electricity, Elsevier Publishing Company, Proceedings of the Third International Conference on Atmospheric and Space Electricity, 1963.

Whipple, E. C., Jr., Doctoral Thesis, The George Washington University, 1965.

Figure Captions

Figure 1

Photograph of Nike-Apache payload showing ion density and solar radiation experiment sensors.

Figure 2

Rocket measurement of (a) positive ion density, N_+ as represented by solid curve, (b) electron density, N_e, as represented by dashed curve.

Figure 3

Photoelectric yield of tungsten as a function of wavelength.

Figure 4

Rocket measurement of unretarded photocurrent from a tungsten target.

Figure 5

The effect of attenuation by the terrestrial atmosphere for specified wavelengths including an experimental and theoretical comparison for the Lyman alpha line.

Figure 6

Total photoionization rate as a function of altitude for specified wavelengths and wavelength bands.

Figure 7

Total ion pair production function and N_+^2 plotted as a function of altitude for the $Z = 58^o$ rocket experiment.

Figure 8

Comparison of positive ion density as measured by two rockets launched at two different solar zenith angles.

Figure 9

Comparison of the square of the positive ion density with the ion pair production function for the D region.